Cancer Letters 455 (2019) 60–72

Contents lists available at ScienceDirect

Cancer Letters

journal homepage: www.elsevier.com/locate/canlet

Original Articles

# A novel hydrogen sulfide-releasing donor, HA-ADT, suppresses the growth of human breast cancer cells through inhibiting the PI3K/AKT/mTOR and Ras/Raf/MEK/ERK signaling pathways

Qian Dong[a,c,1], Bo Yang[a,c,1], Ju-Guo Han[a,c], Meng-Meng Zhang[a,c], Wei Liu[a,c], Xin Zhang[a,c], Hai-Lan Yu[a,c], Zheng-Guo Liu[b,c], Shi-Hui Zhang[a,c], Tao Li[b,c], Dong-Dong Wu[b,c,*], Xin-Ying Ji[b,c,**], Shao-Feng Duan[a,c,***]

[a] Institute for Innovative Drug Design and Evaluation, School of Pharmacy, Henan University, Kaifeng, Henan, 475004, China
[b] School of Basic Medical Sciences, Henan University College of Medicine, Kaifeng, Henan, 475004, China
[c] Henan International Joint Laboratory for Nuclear Protein Regulation, Henan University, Kaifeng, Henan, 475004, China

ARTICLE INFO

*Keywords:*
Hydrogen sulfide
Breast cancer
Apoptosis
Angiogenesis
Signaling pathway

ABSTRACT

Breast cancer is one of the most frequent cancers among women worldwide. Hyaluronic acid (HA) is one of the best biopolymers in terms of safety issues and has been widely used in drug delivery and tissue engineering. 5-(4-hydroxyphenyl)-3*H*-1,2-dithiol-3-thione (ADT-OH) is a commonly used $H_2S$ donor. In this study, we designed and synthesized a conjugate, HA-ADT, by connecting HA with ADT-OH through chemical reactions. Our results indicated that HA-ADT could produce more $H_2S$ than NaHS and GYY4137. HA-ADT exerted more potent inhibitory effects than NaHS and GYY4137 in the proliferation, viability, migration, and invasion of human breast cancer cells. Similar trends were observed in the apoptosis and the protein levels of phospho (p)-PI3K, p-AKT, p-mTOR, H-RAS, p-RAF, p-MEK, and p-ERK in human breast cancer cells. Furthermore, HA-ADT exhibited more powerful inhibitory effects on the growth of human breast cancer xenograft tumors in nude mice. In conclusion, HA-ADT could suppress the growth of human breast cancer cells through the inhibition of the PI3K/AKT/mTOR and RAS/RAF/MEK/ERK signaling pathways. HA-ADT and its derivatives might be of great potential in the treatment of different types of cancer.

## 1. Introduction

Breast cancer is one of the most frequent malignant neoplasms in women worldwide [1–3]. Breast cancer is a heterogeneous disease and comprises many subtypes according to the presence or absence of hormone receptors, namely progesterone receptor, estrogen receptor, and human epidermal growth factor 2 [3–5]. Several factors are known to contribute to the development of breast cancer, including age, reproductive history, genetic factors, and oral contraceptives [2,6]. Recently, the treatment of localized breast cancer is successful with a 5 year survival rate of nearly 90%. However, there is still no effective therapeutic strategy for advanced breast cancer in which metastasis has occurred at the late stage of the cancer, regardless of the use of chemotherapy, radiation, or estrogen blockers [7–9]. Therefore, there is an urgent need to develop novel and effective agents/drugs for the treatment and prevention of breast cancer.

Hydrogen sulfide ($H_2S$) has been widely considered the third gaseous signaling molecule, along with nitric oxide and carbon monoxide [10–12]. An increasing number of studies have shown that $H_2S$ plays important roles in many physiological and pathophysiological functions [10,11,13,14]. $H_2S$ can be endogenously produced in mammals from homocysteine and L-cysteine by two pyridoxal-5′-phosphate (PLP)-dependent enzymes, namely cystathionine β-synthase (CBS) and cystathionine γ-lyase (CSE). 3-mercaptopyruvate sulfurtransferase (3-MST), a PLP-independent enzyme, acts in combination with cysteine aminotransferase to generate $H_2S$ from L-cysteine in the presence of α-ketoglutarate [11,13,15]. Furthermore, a recent study has shown that D-amino acid oxidase can metabolize D-cysteine to an achiral α-ketoacid,

* Corresponding author. School of Basic Medical Sciences, Henan University College of Medicine, Kaifeng, Henan, 475004, China.
** Corresponding author. School of Basic Medical Sciences, Henan University College of Medicine, Kaifeng, Henan, 475004, China.
*** Corresponding author. Institute for Innovative Drug Design and Evaluation, School of Pharmacy, Henan University, Kaifeng, Henan, 475004, China.
*E-mail addresses:* ddwubiomed2010@163.com (D.-D. Wu), 10190096@vip.henu.edu.cn (X.-Y. Ji), dsf_2007@163.com (S.-F. Duan).
[1] Equal contributors.

https://doi.org/10.1016/j.canlet.2019.04.031
Received 21 December 2018; Received in revised form 23 April 2019; Accepted 25 April 2019

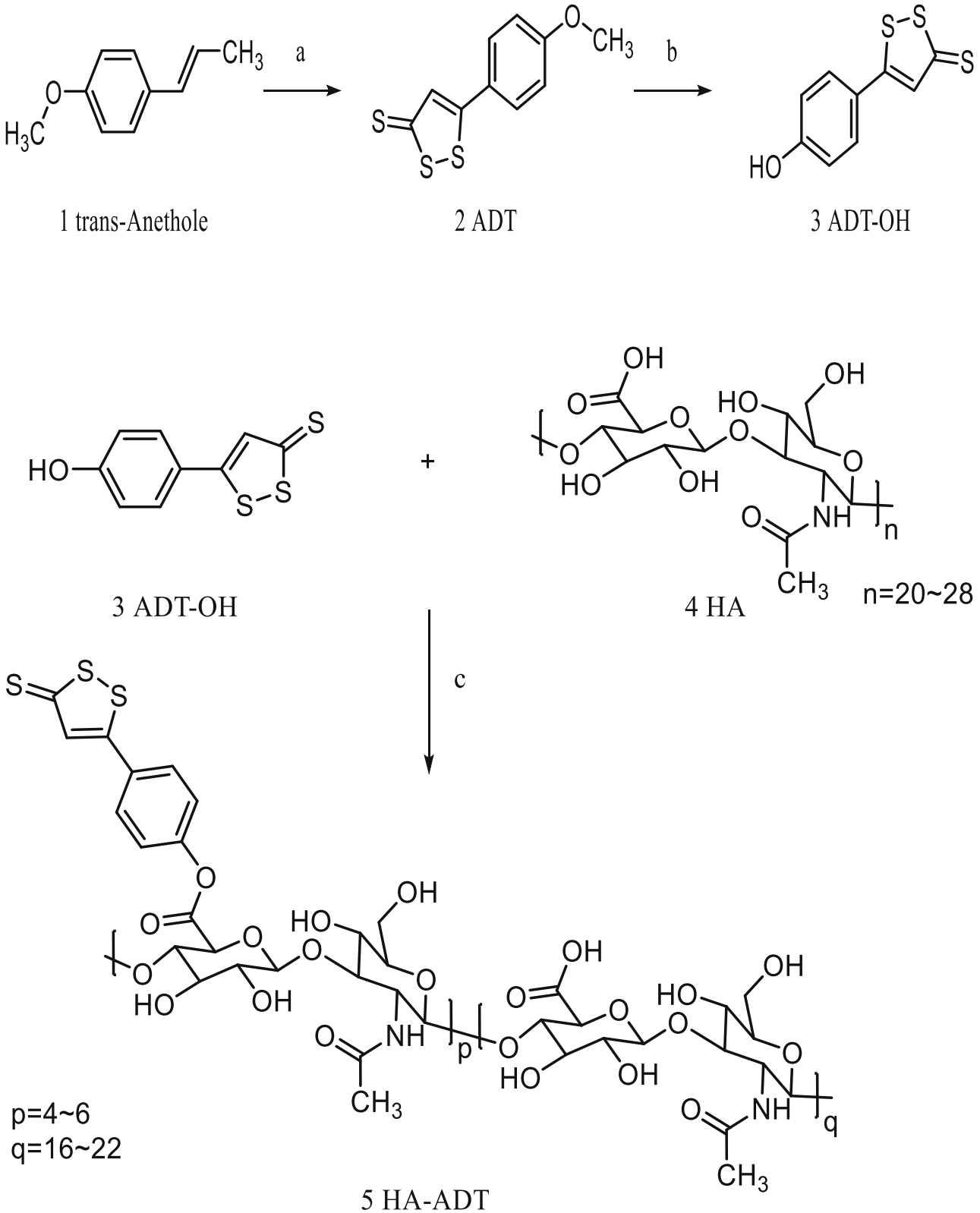


**Fig. 1. Synthesis route of HA-ADT.** Reagents and conditions: (a) S8 AcNMe6, 145 °C, reflux, 6 h; (b) C5H5N·HCl, 215 °C, 20 min, Ar; (c) EDC•HCl/DMAP, DMF/$H_2O$, 0 °C–r.t.

3-mercaptopyruvate, which is further metabolized to $H_2S$ by 3-MST in both brain and kidney [16].

It has been shown that endogenous production of $H_2S$ is generally low, making it difficult to elucidate the precise biological functions [17]. Chemical compounds that could degrade in response to a specific trigger to release $H_2S$, termed $H_2S$ donors, include a number of delivery systems and functional groups, some of which mimic the controlled endogenous production in response to biologically specific and relevant conditions [17]. Hyaluronic acid (HA) is a non-sulfated glycosaminoglycan composed of two disaccharide units, D-glucuronic acid and *N*-

acetyl-D-glucosamine, linked via β-1,3- and β-1,4-glycosidic bonds [18]. HA has been considered one of the best biopolymers in terms of safety issues and widely used for many biomedical applications including tissue engineering and drug delivery [19–21]. 5-(4-hydroxyphenyl)-3*H*-1,2-dithiol-3-thione (ADT-OH), a commonly used $H_2S$ donors, belongs to the class of compounds which possess the 3*H*-1,2-dithiole-3-thione group in their structure [22].

In this study, a novel conjugate, HA-ADT, was designed and synthesized by connecting HA with ADT-OH through chemical reactions. We then detected the mechanism of action of HA-ADT on the proliferation, migration, and invasion of human breast cancer cells *in vitro*. We further examined the effects of HA-ADT on tumor growth in nude mice bearing human breast cancer xenografts.

## 2. Materials and methods

### 2.1. Synthesis of 5-(p-methoxyphenyl)-3H-1,2-dithiolan-3-thione (ADT)

All the chemicals and organic solvents used in this study were obtained from Aladin Chemical Reagent Inc. (Shanghai, China) and used directly without purification or distillation unless otherwise specified. Anethole (8 g, 54 mmol) and sulphur (96.93 g, 377.9 mmol) were refluxed at 145 °C in dimethylacetamide (30 mL) for 6 h. Then the mixture was cooled to room temperature and 100 mL of water ($H_2O$) was added. The whole mixture was extracted with ether (2 × 80 mL). The combined organic phases were washed with brine (100 mL) and $H_2O$ (3 × 100 mL), then dried over sodium sulfate. Removal of the solvent under reduced pressure followed by crystallization using ethyl acetate, yielded the desired compound ADT, the molecular structure of which was verified by $^1$hydrogen-nuclear magnetic resonance ($^1$H NMR).

### 2.2. Synthesis of ADT-OH

Pyridine hydrochloride (32.74 g, 283.28 mmol) was added to ADT (11.33 g, 47.21 mmol) in a dry flask, mixed and then heated to melt at 215 °C under argon protection for 20 min. After being cooled to 100 °C, warmed $H_2O$ (150 mL) was added and hot-filtered. The cake was placed in a beaker and 10% sodium hydroxide (150 mL) was added. The mixture was stirred for 4 h and filtered. Then the cake was dissolved in $H_2O$ (1 L), and the pH was adjusted to 2 with concentrated hydrochloride. The red precipitation was filtered and washed to neutral using $H_2O$, then dried in a vacuum desiccator to yield a compound. The structure of the synthetic molecule was determined by $^1$H NMR.

### 2.3. Synthesis of HA-ADT

HA (1.5 g, 3.98 mmol) was dissolved in N,N-Dimethylformamide (DMF)/distilled water (dd$H_2O$) (1:1, v/v). After the homogeneous solution was formed, 1-Ethyl-3-(3-dimethylaminopropyl)carbodiimide hydrochloride (0.76 g, 3.96 mmol) and 4-dimethylaminopyridine (0.16 g, 1.33 mmol) were added and the temperature was kept at 0 °C. After 1 h, the DMF solution of ADT-OH (0.6 g, 2.66 mmol) was added. The reaction was proceeded at 0 °C for 30 min and then at room temperature overnight. The crude product was dialyzed against DMF for 5 h, then dialyzed against DMF/dd$H_2O$ (1/1, v/v) for 10 h and $H_2O$ for 2 days using 3.5 kDa dialysis tubing. The supernatant was filtered through a 0.45 μm pore-sized microporous membrane and freeze-dried to obtain the HA-ADT (Fig. 1). The molecular structure and grafting ratio were determined by $^1$H NMR.

### 2.4. Cell culture

Human normal breast cell line MCF-10A and human breast cancer cell lines MCF-7 and MDA-MB-231 were purchased from Nanjing Kebai Biological Technology Co., Ltd. (Nanjing, Jiangsu, China). MCF-7 cells were cultured in RPMI 1640 medium supplemented with 10% fetal bovine serum (FBS), 100 U/ml penicillin, and 100 μg/mL streptomycin. MCF-10A and MDA-MB-231 cells were cultured in Dulbecco's modified Eagle's medium supplemented with 10% FBS, 100 U/ml penicillin, and 100 μg/mL streptomycin. Cells were grown in an incubator with a humidified atmosphere of 95% air and 5% $CO_2$ at 37 °C. Cells were treated with 200 μM NaHS, 200 μM GYY4137, and 200 μM HA-ADT, respectively. The control group was treated with PBS. After 24 h of treatment, the cells were then used for subsequent experiments.

### 2.5. Cell growth assay

The CCK-8 detection kit (Beyotime Institute of Biotechnology, Shanghai, China) was used to measure cell viability according to the manufacturer's instructions [23]. The 5-Ethynyl-2-deoxyuridine (EdU) staining assay was performed using the Cell-Light EdU Apollo 567 In Vitro Imaging Kit (RiboBio, Guangzhou, Guangdong, China) according to the manufacturer's instructions. Cell proliferation rate (%) = (EdU-positive cells)/(total number of cells) × 100 [24].

### 2.6. Wound healing assay

Confluent cells were scratched using a sterile micropipette tip and washed twice with PBS. The migration distance was observed and photographed under an Olympus CKX41 microscope and then measured using Image J software (National Institute for Health, Bethesda, MD, USA). The cell migration rate (MR) was calculated: MR (%) = [(A − B)/A] × 100, where A is the width at 0 h, and B is the width at 24 h [25].

### 2.7. TdT-mediated dUTP-biotin nick end labeling (TUNEL) assay

TUNEL assay was performed using the In Situ Cell Death Detection Kit (Beyotime Biotechnology, Shanghai, China) according to the manufacturer's instructions. The stained cells were observed using a fluorescent microscope (Eclipse Ti, Nikon, Melville, NY, USA). The percentage of positive cells was calculated using Image J software.

### 2.8. Measurement of $H_2S$ levels

NaHS, GYY4137, and HA-ADT were separately dissolved in the culture supernatant of MCF-10A, MCF-7, and MDA-MB-231 cells with a final concentration of 200 μM. Then the concentration of $H_2S$ was separately determined at 0.3, 0.6, 1, 3, 6, 12, 24, and 48 h. In addition, 200 μM NaHS, GYY4137, and HA-ADT was added to the culture medium, the concentrations of $H_2S$ in both cells and culture supernatant at 48 h were determined. The $H_2S$ level was measured by using enzyme-linked immunosorbent assay (ELISA) kits according to the manufacturer's protocols (LanpaiBio, Shanghai, China). Briefly, the cells and culture supernatant were collected to test the levels of $H_2S$. Then, the standard controls were diluted, in which the concentration of $H_2S$ was 3, 6, 12, 24, and 48 nmol/mL, respectively. The samples were diluted and incubated for 0.5 h at 37 °C. After $H_2S$ was bound and the plates were washed, the conjugate reagent was added to the well and incubated for 0.5 h at 37 °C. After washing, the color-developing agents were added to each well and incubated for 15 min at 37 °C. The optical density of each well was measured using a microplate reader (Bio-Rad, CA, USA) at 450 nm. A standard curve was generated by plotting the logarithm of the mean absorbance for each standard versus the logarithm of the known $H_2S$ concentration. The value for the blank was subtracted from both the samples and the standard controls.

### 2.9. Colony formation assay

Cells were treated with PBS, 200 μM NaHS, 200 μM GYY4137, and 200 μM HA-ADT respectively for 24 h. Then cells ($1 \times 10^3$ per well) were seeded in 6-well plates and cultivated in culture medium for two

weeks at 37 °C. The colonies were washed with PBS buffer before methanol fixation for 15 min, and crystal violet was added and incubated for 30 min at room temperature. The plates were washed with distilled water and air-dried. Then the plates were scanned for counting the number of colonies.

### 2.10. Soft agar assay

Cells were suspended in 0.6% agarose and medium supplemented with 10% FBS, and the mixture was seeded in 6-well plates ($1 \times 10^4$ per well) containing a basal layer of 1.2% agarose. Cells were treated with PBS, 200 μM NaHS, 200 μM GYY4137, and 200 μM HA-ADT respectively for 24 h. The culture medium was replaced twice a week. After two weeks, colonies were visualized and photographed under an Olympus CKX41 microscope. Colonies larger than 0.1 mm in diameter were counted.

### 2.11. Migration and invasion assays

$1 \times 10^5$ cells in serum-free medium were seeded onto the upper chamber uncoated or coated with Matrigel (BD Biosciences, San Jose, CA, USA). In addition, the medium containing 10% FBS was added to the lower chamber. After treatment with PBS, 200 μM NaHS, 200 μM GYY4137, and 200 μM HA-ADT respectively for 24 h, the cells remaining on the upper side were scrubbed off with cotton swabs, while cells on the bottom of the membrane were fixed with 4% paraformaldehyde and then stained with 0.1% crystal violet. The number of cells was counted under a Zeiss Axioskop 2 plus microscope (Carl Zeiss, Thornwood, NY, USA).

### 2.12. Western blotting

After treatment with PBS, 200 μM NaHS, 200 μM GYY4137, and 200 μM HA-ADT respectively for 24 h, total protein was extracted from MCF-7 and MDA-MB-231 cells. Western blotting was performed to determine the expression levels of target proteins. The primary antibodies, including anti-H-RAS, anti-RAF, anti-phospho (p)-c-RAF (Ser259), anti-MEK1/2, anti-p-MEK1/2 (Ser217/221), anti-extracellular signal-regulated protein kinase 1/2 (ERK1/2), anti-p-ERK1/2 (Thr202/Tyr204), anti-phosphatidylinositol 3-kinase (PI3K), anti-p-PI3K (Tyr458/Tyr199), anti-Akt, anti-p-Akt (Ser473), anti-mammalian target of rapamycin (mTOR), and anti-p-mTOR (Ser2448) antibodies were purchased from Cell Signaling Technology (CST, Danvers, MA, USA). Anti-B-cell lymphoma-2 (Bcl-2), anti-Bcl-2-associated X protein (Bax), anti-B-cell lymphoma-extra large (Bcl-xl), anti-Bcl-xl/Bcl-2-associated death promoter (Bad), anti-caspase-3 (Cas-3), anti-cleaved Cas-3, anti-caspase-9 (Cas-9), anti-cleaved Cas-9, anti-poly adenosine diphosphate-ribose polymerase (PARP), anti-cleaved PARP, and anti-β-actin antibodies were purchased from ProteinTech (Chicago, IL, USA). The horseradish peroxidase-conjugated secondary antibody was purchased from CST. The reaction was visualized by an enhanced chemiluminescence system (Thermo Fisher Scientific, Rockford, IL, USA). The bands were semi-quantified using Image J software. The results were normalized to the expression level of β-actin.

### 2.13. Animal study

Animal experiments were approved by the Committee of Medical Ethics and Welfare for Experimental Animals of Henan University School of Medicine (HUSOM-2017-195) in compliance with the Experimental Animal Regulations formulated by the National Science and Technology Commission, China. Animal studies were conducted as previously described with slight modifications [25]. Forty-eight 4-week-old male BALB/C nude mice were purchased from Beijing Vital River Laboratory Animal Technology Co., Ltd. (Certificate No. SCXK (Jing) 2011-0011, Beijing, China). MCF-7 and MDA-MB-231 cells ($5 \times 10^6$ cells in 200 μL PBS) were implanted by subcutaneous injection into the right flanks of mice. At 24 h after inoculation, the mice were randomly divided into four groups (n = 6 per group). Then PBS, 200 μM NaHS, 200 μM GYY4137, and 200 μM HA-ADT were subcutaneously administered (near the implanted tumor) once a day for 14 days. During the experiment, the mice were weighed and the tumor volumes were measured daily. The tumor volumes were calculated as volume (V) = $L \times W^2/2$, where L is the longest dimension parallel to the skin surface and W is the dimension perpendicular to L and parallel to the surface [26]. The tumor volume doubling time (TVDT) was calculated as TVDT = $(T - T_0) \times \log2/\log(V2/V1)$, where $(T - T_0)$ represents the time interval and V2 and V1 indicate the volumes of tumor at the two measurement times [27]. At the end of the experiment, mice were sacrificed and tumors were excised and weighted to determine the inhibition rate (IR). The IR of tumor growth was calculated as IR (%) = [(A - B)/A] × 100, where A is the average tumor weight of the control group, and B is that of the treatment group [28].

### 2.14. Hematoxylin and eosin (HE) staining

After the mice were sacrificed, a necropsy examination was immediately performed. Tumor samples were fixed in 10% neutral buffered formalin and embedded in paraffin. Then the samples were sectioned at 5 μm thickness and stained with HE. Tumor tissues were observed under a Zeiss Axioskop 2 plus microscope.

### 2.15. Immunohistochemistry (IHC) and evaluation

Tumor tissues were stained with anti-Ki67 antibody (CST, Danvers, MA, USA) and Ki67-positive cells were photographed using a Zeiss Axioskop 2 plus microscope. The proliferation index (PI) was determined by the percentage of the Ki67 positive cells out of the total number of tumor cells [24,29]. Cluster of differentiation 31 (CD31) is an ideal biomarker for vascular endothelial cells, and its immunostaining density is represented by the microvessel density (MVD) [25,30]. Tumor tissues were stained by IHC using CD31 antibody (CST, Danvers, MA, USA) to determine the tumor MVD. Stained vessels with a clearly defined lumen or well-defined linear vessel shape were photographed under a Zeiss Axioskop 2 plus microscope and counted from the representative tumor zone.

### 2.16. Statistical analysis

Data are presented as mean ± standard error of the mean. The differences between multiple groups were analyzed by one-way analysis of variance using SPSS 17.0 software, followed by Tukey's test. A P value of less than 0.05 was considered to be statistically significant.

## 3. Results

### 3.1. Synthesis of HA-ADT

ADT was a yellow solid (11.33 g, yield 81.8%) M. p. 110-110 °C. $^1$H NMR (DMSO-$d_6$, 300 MHz): δ = 7.88 (d, $J$ = 8.1 Hz, 2H, Ar-H), 7.77 (s, 1H, = CH), 7.08 (d, $J$ = 7.7 Hz, 2H, Ar-H), 3.86 (s, 3H, -OCH3) (Supplementary Fig. S1). ADT-OH was an orange solid (8.43 g, yield 79%) M. p. 191–192 °C. $^1$H NMR (DMSO-$d_6$, 300 MHz): δ = 10.53 (s, 1H, -OH), 7.78 (d, $J$ = 8.8 Hz, 2H, Ar-H), 7.71 (s, 1H, = CH), 6.91 (d, $J$ = 8.7 Hz, 2H, Ar-H) (Supplementary Fig. S3). In addition, LCMS was also performed for ADT and ADT-OH, showing that they were pure enough (Supplementary Figs. S2 and S4). After dialysis and lyophilization, the desired product was successfully obtained as an orange solid, which was then characterized via $^1$H NMR ($D_2O$, 300 MHz): δ = 1.89 (s, NHCOCH3), 1.0–4.4 (m, HA-H), 6.76 (d, Ar-H), 7.80 (s, = CH), 7.88 (d, Ar-H) (Supplementary Fig. S5). The grafting ratio of ADT-OH onto HA was 25% by comparing the integration of one aromatic

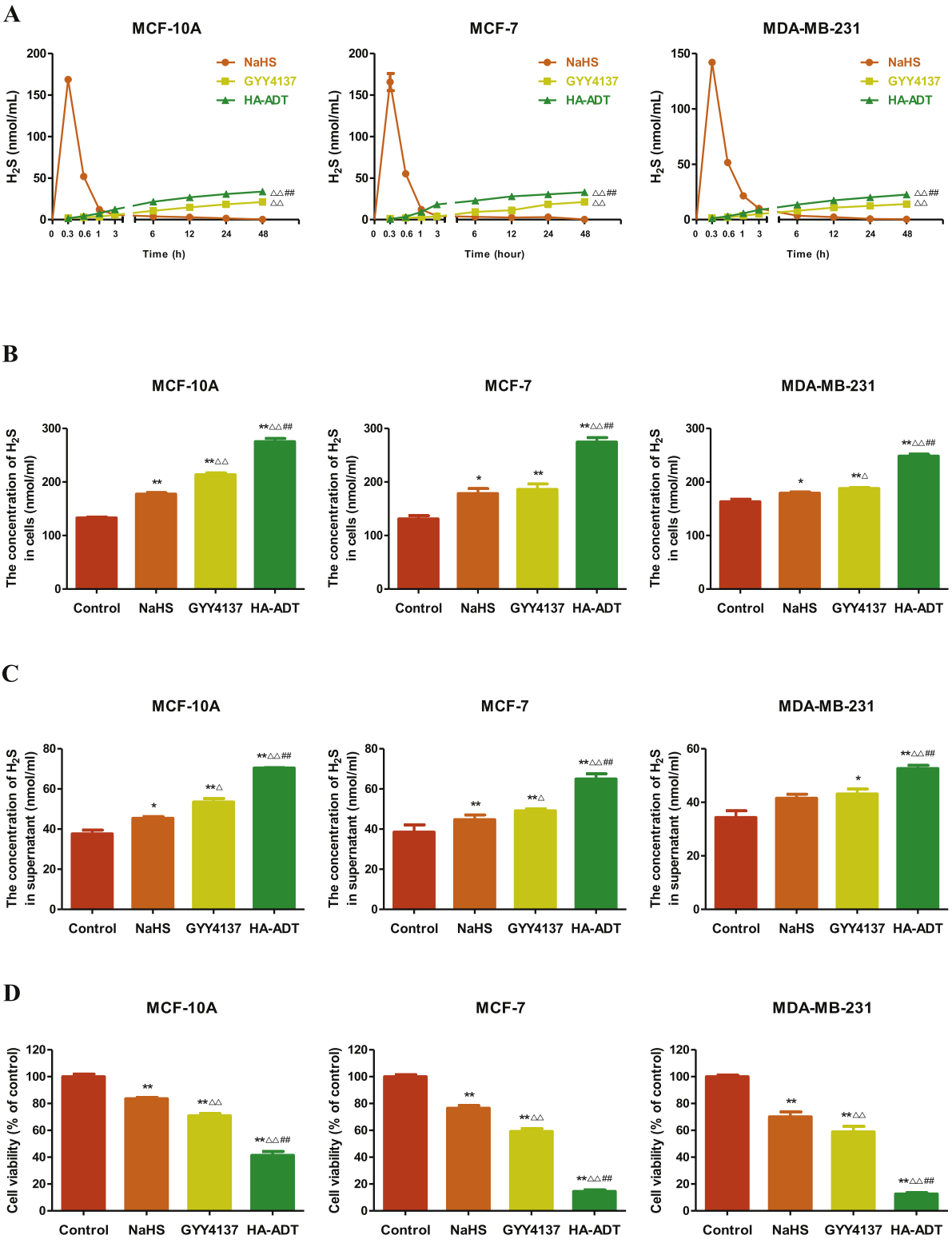


**Fig. 2. $H_2S$-releasing profile of HA-ADT and the effects of HA-ADT on the viability of human breast cancer cells. (A)** NaHS, GYY4137, and HA-ADT were separately dissolved in the culture supernatant of MCF-10A, MCF-7, and MDA-MB-231 cells with a final concentration of 200 μM. The concentration of $H_2S$ was separately determined at 0.3, 0.6, 1, 3, 6, 12, 24, and 48 h. Then 200 μM NaHS, GYY4137, and HA-ADT was separately added to the culture medium, the concentrations of $H_2S$ in both cells **(B)** and culture supernatant **(C)** at 48 h were determined. **(D)** The percentages of viable cells were determined using CCK-8 assay and the cell viability of the control group was taken as 100%. Data are presented as mean ± SEM of three independent experiments; $^{*}P < 0.05$, $^{**}P < 0.01$ compared with the control group; $^{\triangle}P < 0.05$, $^{\triangle\triangle}P < 0.01$ compared with NaHS group; $^{\#\#}P < 0.01$ compared with GYY4137 group.

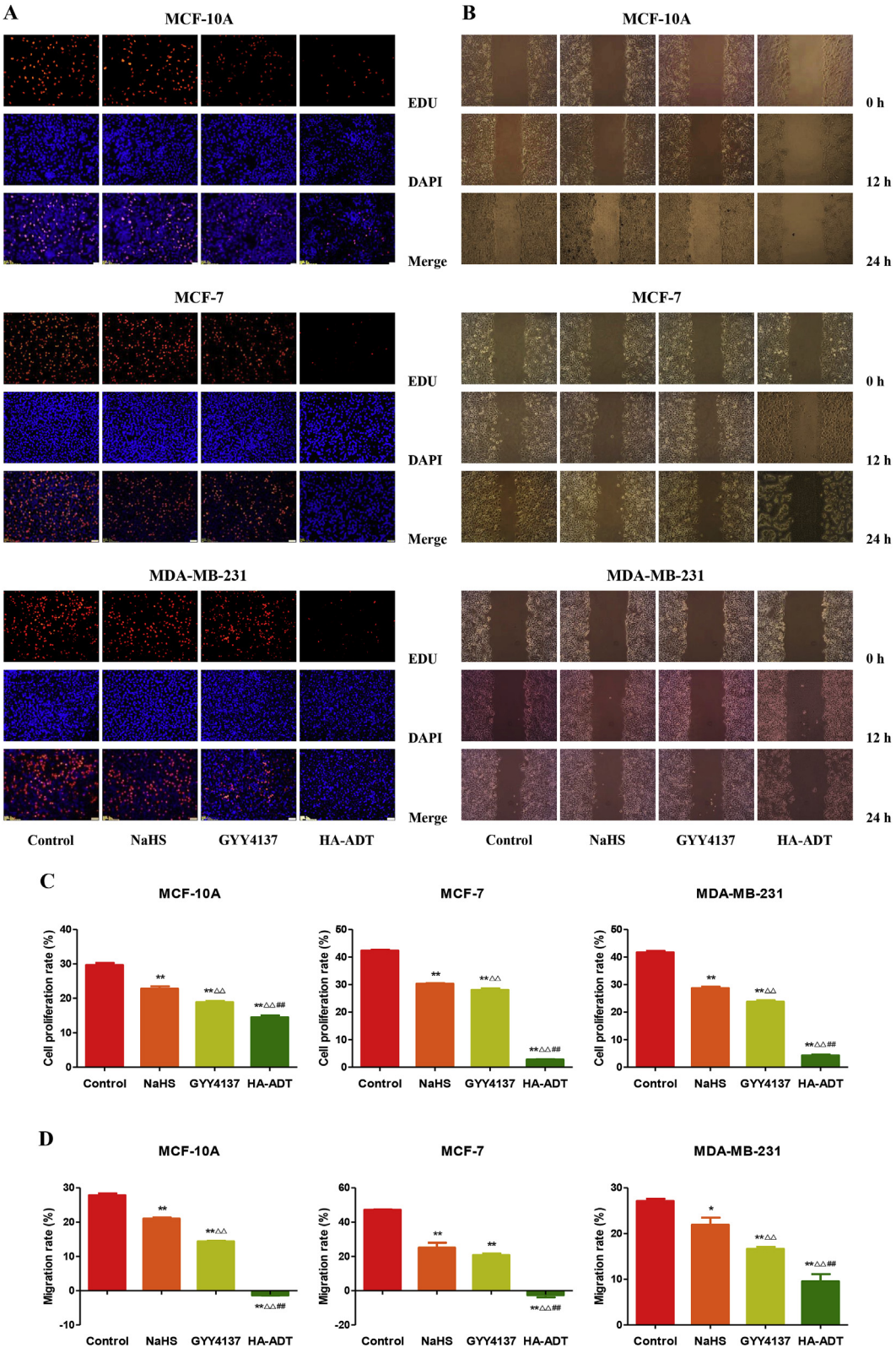


**Fig. 3. Effects of HA-ADT on the proliferation and healing ability of human breast cancer cells. (A)** DNA replication activities of MCF-10A, MCF-7, and MDA-MB-231 cells in each group were examined by EdU assay; original magnification 100×. **(B)** The effect of HA-ADT on cell migration was measured by wound healing assay; original magnification 100×. **(C)** The proliferation rate of each group was analyzed. **(D)** The migration rates of MCF-10A, MCF-7, and MDA-MB-231 cells were calculated by the formula shown above. Data are presented as mean ± SEM of three independent experiments; $^{*}P < 0.05$, $^{**}P < 0.01$ compared with the control group; $^{\triangle\triangle}P < 0.01$ compared with NaHS group; $^{\#\#}P < 0.01$ compared with GYY4137 group.

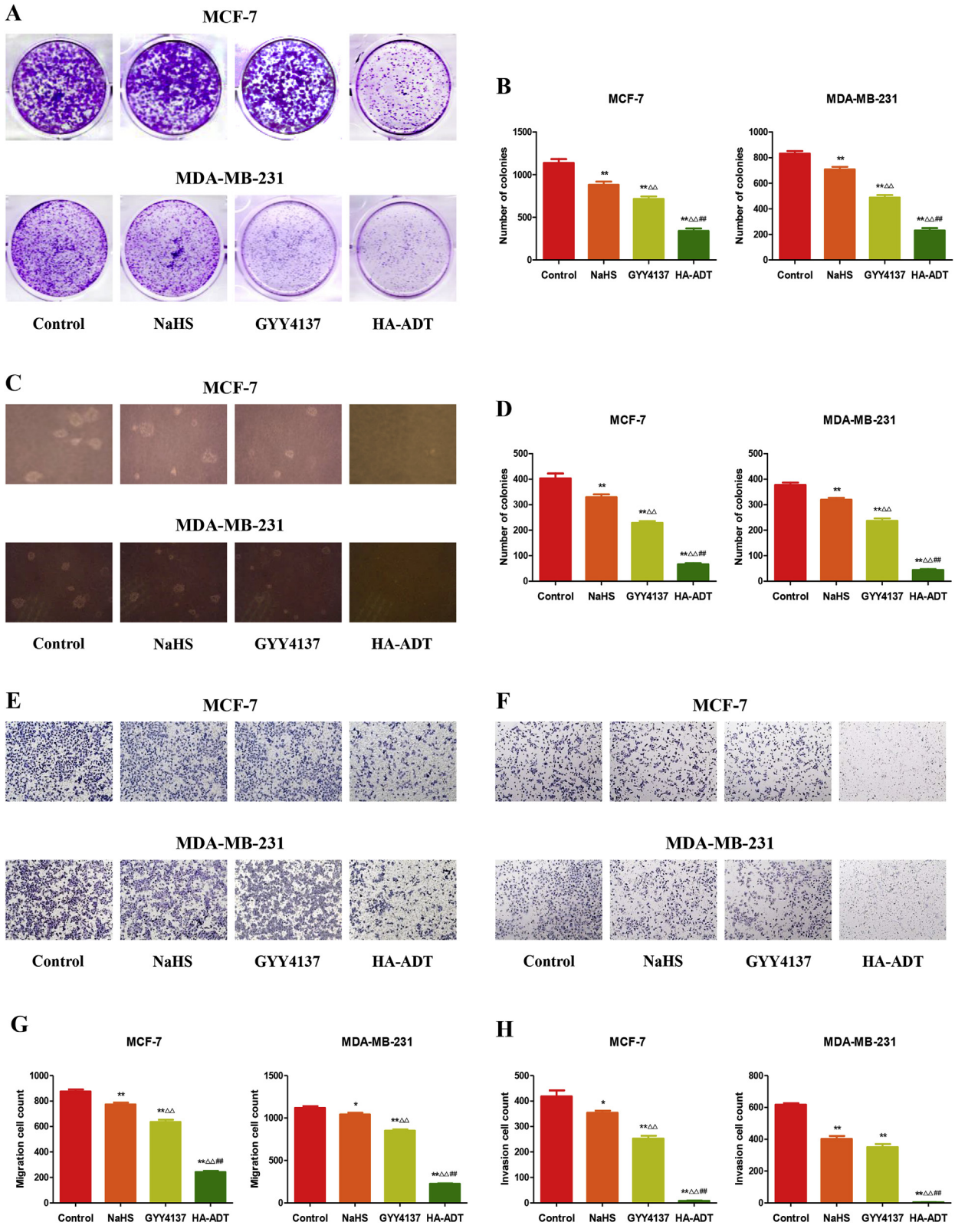


**Fig. 4. Effects of HA-ADT on the migration and invasion of human breast cancer cells. (A)** The clonogenic capacity was determined in MCF-7 and MDA-MB-231 cells. **(B)** The numbers of colonies were calculated. **(C)** Soft agar assay was performed to examine the anchorage-independent survival of cells; original magnification 100×. **(D)** The number of colonies was calculated. **(E)** Transwell assay was performed to assess the migration of MCF-7 and MDA-MB-231 cells; original magnification 200×. **(F)** Transwell assay was performed to assess the invasion of MCF-7 and MDA-MB-231 cells; original magnification 200×. **(G)** The numbers of the migrated cells were calculated. **(H)** The numbers of the invasive cells were calculated. Data are presented as mean ± SEM of three independent experiments; $^{*}P < 0.05$, $^{**}P < 0.01$ compared with the control group; $^{\triangle\triangle}P < 0.01$ compared with NaHS group; $^{\#\#}P < 0.01$ compared with GYY4137 group.

hydrogen to that of the methyl group on HA.

### 3.2. HA-ADT decreases the growth, migration, and invasion of human breast cancer cells

The levels of $H_2S$ in HA-ADT group were higher than those in control, NaHS, and GYY4137 group in MCF-10A, MCF-7, and MDA-MB-231 cells, as well as in the supernatant (Fig. 2A–C). These results suggest that HA-ADT could release more $H_2S$ than NaHS and GYY4137. As shown in Fig. 2D, HA-ADT significantly decreased the viability of MCF-10A, MCF-7, and MDA-MB-231 cells, when compared to the control, NaHS, and GYY4137 group. HA-ADT showed similar effects on the proliferation and migration capabilities of MCF-10A, MCF-7, and MDA-MB-231 cells (Fig. 3). In addition, HA-ADT reduced the colony formation in MCF-7 and MDA-MB-231 cells (Fig. 4A and B). In soft agar assay, HA-ADT decreased the anchorage-independent growth of MCF-7 and MDA-MB-231 cells (Fig. 4C and D). Furthermore, treatment with HA-ADT exhibited impaired migration and invasion capacities in MCF-7 and MDA-MB-231 cells (Fig. 4E–H). Taken together, these results indicate that HA-ADT could decrease the growth, migration, and invasion of human breast cancer cells.

### 3.3. HA-ADT induces apoptosis of human breast cancer cells

As shown in Fig. 5A and B, the apoptotic index increased in the HA-ADT group compared with the control, NaHS, and GYY4137 group. The ratio between Bad and Bcl-xl and the ratio between Bax and Bcl-2 have been regarded as important factors in the regulation of apoptosis. Increased Bad/Bcl-xl and Bax/Bcl-2 ratios are common phenomena in mitochondrial apoptosis in mammals [31,32]. As shown in Fig. 5C–E, Bad/Bcl-xl and Bax/Bcl-2 ratios increased in the HA-ADT group compared with the control, NaHS, and GYY4137 group. The protein levels of cleaved cas-3, 9, and cleaved PARP in human breast cancer cells exhibited similar trends. The results show that HA-ADT could induce apoptosis of human breast cancer cells.

### 3.4. HA-ADT blocks the PI3K/AKT/mTOR and Ras/Raf/MEK/ERK signaling pathways in human breast cancer cells

The PI3K/Akt/mTOR signaling pathway is a key signal transduction pathway involved in many hallmarks of cancer, including survival, metabolism, motility, and genomic instability [33,34]. The pathway contributes to several cancer-promoting aspects of the tumor environment, such as angiogenesis and inflammatory cell recruitment [33]. As shown in Fig. 6A–C, phosphorylations of PI3K, AKT, and mTOR were decreased in HA-ADT group compared with the control, NaHS, and GYY4137 group. The RAS/RAF/MEK/ERK signaling cascade plays an important role in the regulation of a number of cellular processes, including survival, proliferation, differentiation, apoptosis, motility, and metabolism [35,36]. Deregulation of the RAS/RAF/MEK/ERK cascade is a hallmark for driving tumorigenesis in many types of human cancers [37,38]. As shown in Fig. 6D–F, the protein levels of H-RAS, p-RAF, p-MEK, and p-ERK were decreased in HA-ADT group compared with the control, NaHS, and GYY4137 group. In sum, these results suggest that HA-ADT could block the PI3K/AKT/mTOR and Ras/Raf/MEK/ERK signaling pathways in human breast cancer cells.

### 3.5. HA-ADT inhibits the growth and angiogenesis of human breast cancer xenograft tumors in nude mice

Human MCF-7 and MDA-MB-231 breast cancer cells have been widely adopted to establish subcutaneous xenograft models [39,40]. Therefore, the effect of HA-ADT on the growth of breast cancer xenograft tumors was determined. HA-ADT decreased the growth of xenograft tumors, when compared to the control, NaHS, and GYY4137 group (Fig. 7A–E). There were no significant differences in relative weights of heart, liver, spleen, lung, kidney, and brain (Supplementary Tables S1 and S2). In addition, there was no significant difference in body weight between each group (Fig. 7F and G). Ki67, a nuclear non-histone protein, is an important proliferative marker and has been widely used in detecting the proliferation of cancer cells [24,29]. IHC with the Ki67 antibody confirmed that the *in vivo* proliferation of breast cancer cells was inhibited in the HA-ADT group compared with the control, NaHS, and GYY4137 group. CD31 has been regarded as an ideal biomarker for vascular endothelial cells and its density is widely used as the tumor MVD [25,30]. The expression level of CD31 in breast cancer xenograft tumors showed a similar trend (Fig. 7H–L). These results together demonstrate that HA-ADT could inhibit the growth and angiogenesis of human breast cancer xenograft tumors.

## 4. Discussion

$H_2S$ has been regarded as the third gaseous signaling molecule involved in a wide range of physiological and pathological conditions [10–14]. Our previous study has indicated that endogenous $H_2S$ or relatively low levels of exogenous $H_2S$ may maintain or promote cancer cell growth, whereas overexpression of $H_2S$-generating enzymes or treatment with relatively high concentrations of $H_2S$ donor can exhibit anti-cancer effects [41]. HA, a non-sulfated glycosaminoglycan composed of two disaccharide units, is one of the best biopolymers in terms of safety issues and widely used for biomedical applications including drug delivery and tissue engineering [18–21]. ADT-OH, a commonly used $H_2S$ donors, is one of the compounds which possess the 3*H*-1,2-dithiole-3-thione group in their structure [22]. In the present study, we designed and synthesized HA-ADT by connecting HA with ADT-OH through chemical reactions.

Breast cancer is one of the most frequent malignancies diagnosed in women all over the world [1–3]. Recently, there is no effective therapeutic strategy for advanced breast cancer in which metastasis has occurred at the late stage of the cancer [7–9]. Therefore, it is urgent to develop novel and effective agents/drugs for the treatment and prevention of breast cancer. In this study, we investigated the mechanism of action of HA-ADT on the growth of human breast cancer cells both *in vitro* and *in vivo*. The results indicated that HA-ADT could release more $H_2S$ than NaHS and GYY4137. In addition, HA-ADT exhibited more potent effects than NaHS and GYY4137 on inhibiting the proliferation and viability, as well as reducing the migration and invasion capabilities of human breast cancer cells, suggesting that HA-ADT could play an important role in attenuating the growth, migration, and invasion of human breast cancer cells. However, HA-ADT showed toxicity to normal human breast cells. Generally, conventional chemotherapies mainly focus on mass cell killing with low specificities and may result in a wide range of side effects such as toxicity [41,42]. Recent studies have revealed that glycoconjugation is a promising approach for specific targeting of cancer, which could improve therapeutic effects and reduce toxicities of antitumor drugs/agents [43–45]. Therefore, we hypothesize that the toxicity of HA-ADT will possibly be reduced via glycolconjugation. Novel antitumor conjugates can be further prepared to investigate their therapeutic effects in cancer, such as HA-glucose-ADT.

Apoptosis is crucial for the maintenance of tissue homeostasis and normal development in multicellular organisms [46]. There are two major apoptotic signaling pathways: the intrinsic mitochondria-mediated pathway and the extrinsic death receptor-induced pathway [47]. Apoptosis can be regulated by many Bcl-2 family proteins, including antiapoptotic proteins such as Bcl-xl and Bcl-2, as well as proapoptotic proteins such as Bad and Bax [48]. Caspases are activated by diverse apoptotic stimuli and PARP can be further cleaved by activated caspase-3, resulting in the occurrence of apoptotic cascade [25]. A novel $H_2S$-releasing derivative of naproxen, 2-(6-methoxynapthalen-2-yl)-propionic acid 4-thiocarbamoyl phenyl ester, could induce apoptosis of human melanoma A375 cells in a time-dependent manner, which can be confirmed by the cleavage of caspase 3 and PARP [49]. Similarly,

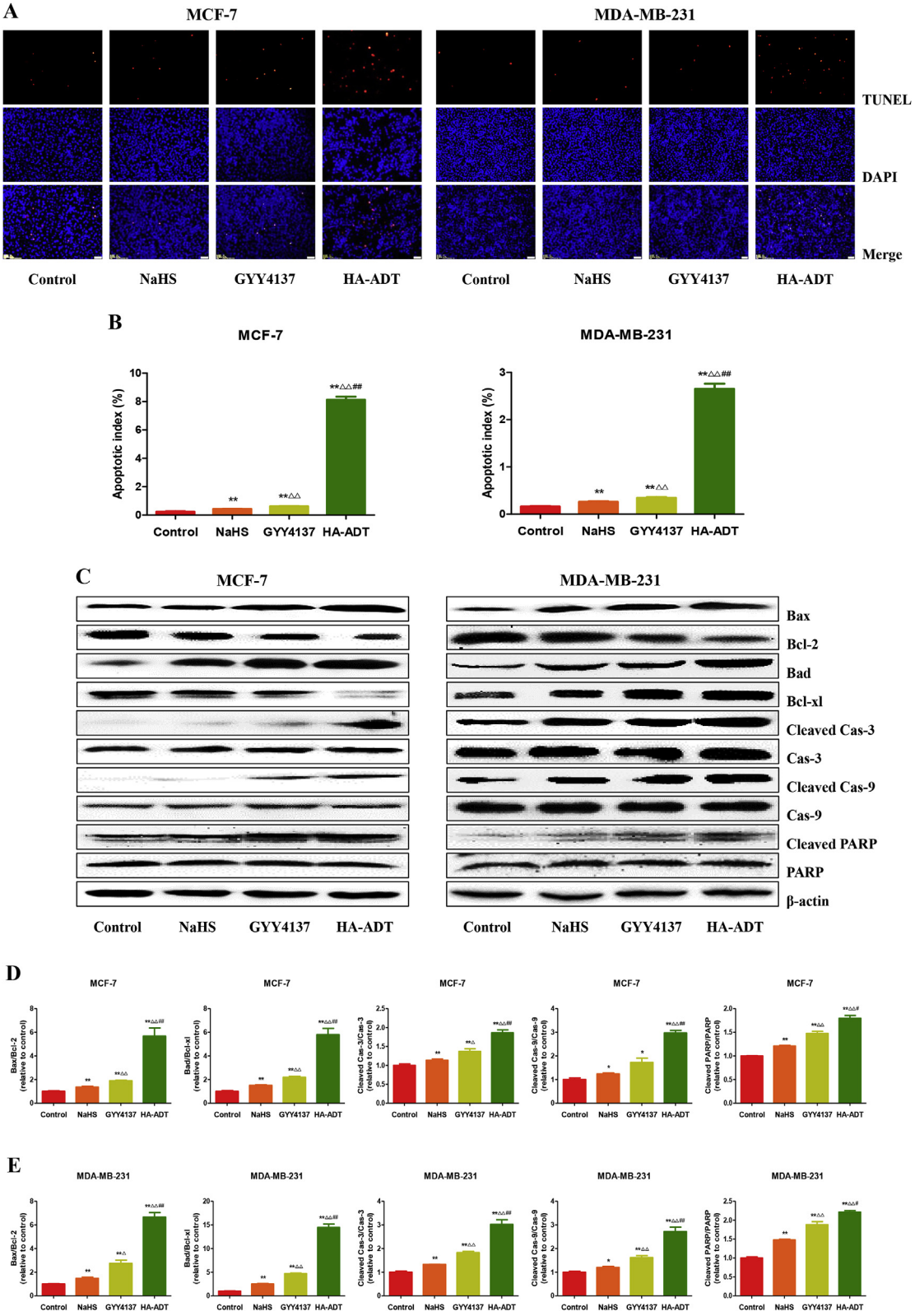


**Fig. 5. Effects of HA-ADT on the apoptosis of human breast cancer cells. (A)** The apoptotic levels were measured by TUNEL staining; original magnification 100×. **(B)** The percentages of TUNEL-positive cells were calculated by the formula: the apoptotic index = (positively stained apoptotic cells)/(total number of cells) × 100%. **(C)** Western blotting analysis for the expression levels of Bax, Bcl-2, Bad, Bcl-xl, cleaved cas-3, cas-3, cleaved cas-9, cas-9, cleaved PARP, and PARP in each group. β-actin was used as the loading control. **(D,E)** The densitometry analysis of each factor was performed in each group, normalized to the corresponding β-actin level. Data are presented as mean ± SEM of three independent experiments; $^{*}P < 0.05$, $^{**}P < 0.01$ compared with the control group; $^{\triangle}P < 0.05$, $^{\triangle\triangle}P < 0.01$ compared with NaHS group; $^{\#}P < 0.05$, $^{\#\#}P < 0.01$ compared with GYY4137 group.

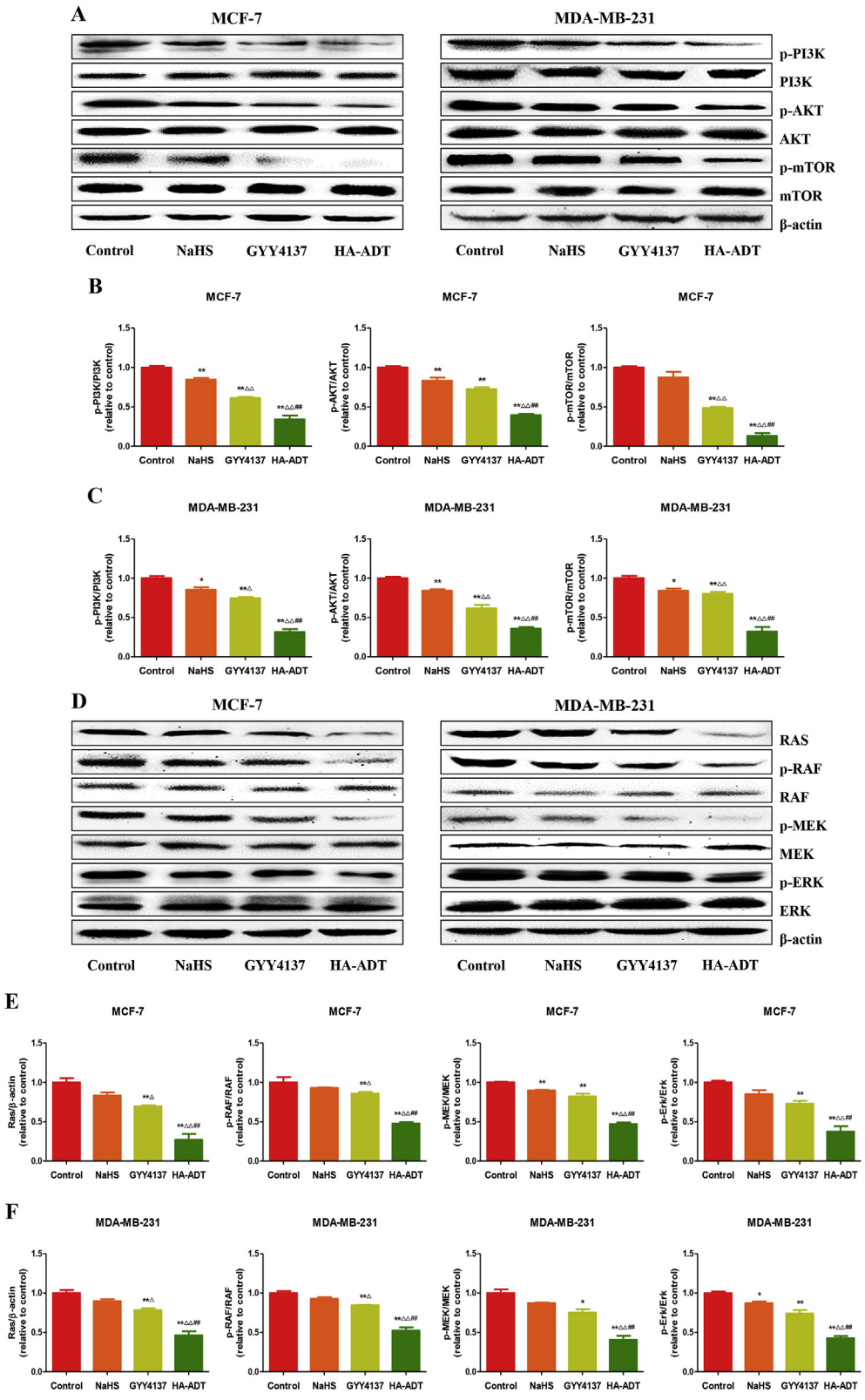


**Fig. 6. Effects of HA-ADT on the PI3K/AKT/mTOR and Ras/Raf/MEK/ERK signaling pathways in human breast cancer cells. (A)** Western blotting analysis for the expression levels of p-PI3K, PI3K, p-AKT, AKT, p-mTOR, and mTOR in MCF-7 and MDA-MB-231 cells. β-actin was used as the loading control. **(B,C)** The densitometry analysis of each factor was performed in each group, normalized to the corresponding β-actin level. **(D)** Western blotting analysis for the expression levels of RAS, p-RAF, RAF, p-MEK, MEK, p-ERK, and ERK in MCF-7 and MDA-MB-231 cells. β-actin was used as the loading control. **(E,F)** The densitometry analysis of each factor was performed in each group, normalized to the corresponding β-actin level. Data are presented as mean ± SEM of three independent experiments; $^{*}P < 0.05$, $^{**}P < 0.01$ compared with the control group; $^{\triangle}P < 0.05$, $^{\triangle\triangle}P < 0.01$ compared with NaHS group; $^{\#\#}P < 0.01$ compared with GYY4137 group.

our results indicated that HA-ADT can increase the apoptotic index in human breast cancer cells via up-regulation of the protein levels of cleaved cas-3, 9, and cleaved PARP, suggesting the activation of mitochondria-mediated pathway.

The PI3K/AKT/mTOR pathway is involved in the regulation of cell growth, survival, motility, and protein synthesis [25,50]. It has been shown that activation of the pathway contributes to tumor progression and reduced patient survival [51]. The RAS/RAF/MEK/ERK pathway is active in different types of human cancers and plays crucial roles in cancer development and progression [52]. An increasing number of studies reveal that the PI3K/AKT/mTOR and the RAS/RAF/MEK/ERK pathway have a synergetic relationship in regulating the proliferation of cancer cells [53–55]. Dual inhibition of both pathways have shown favorable efficacy compared with inhibition of either pathway in the

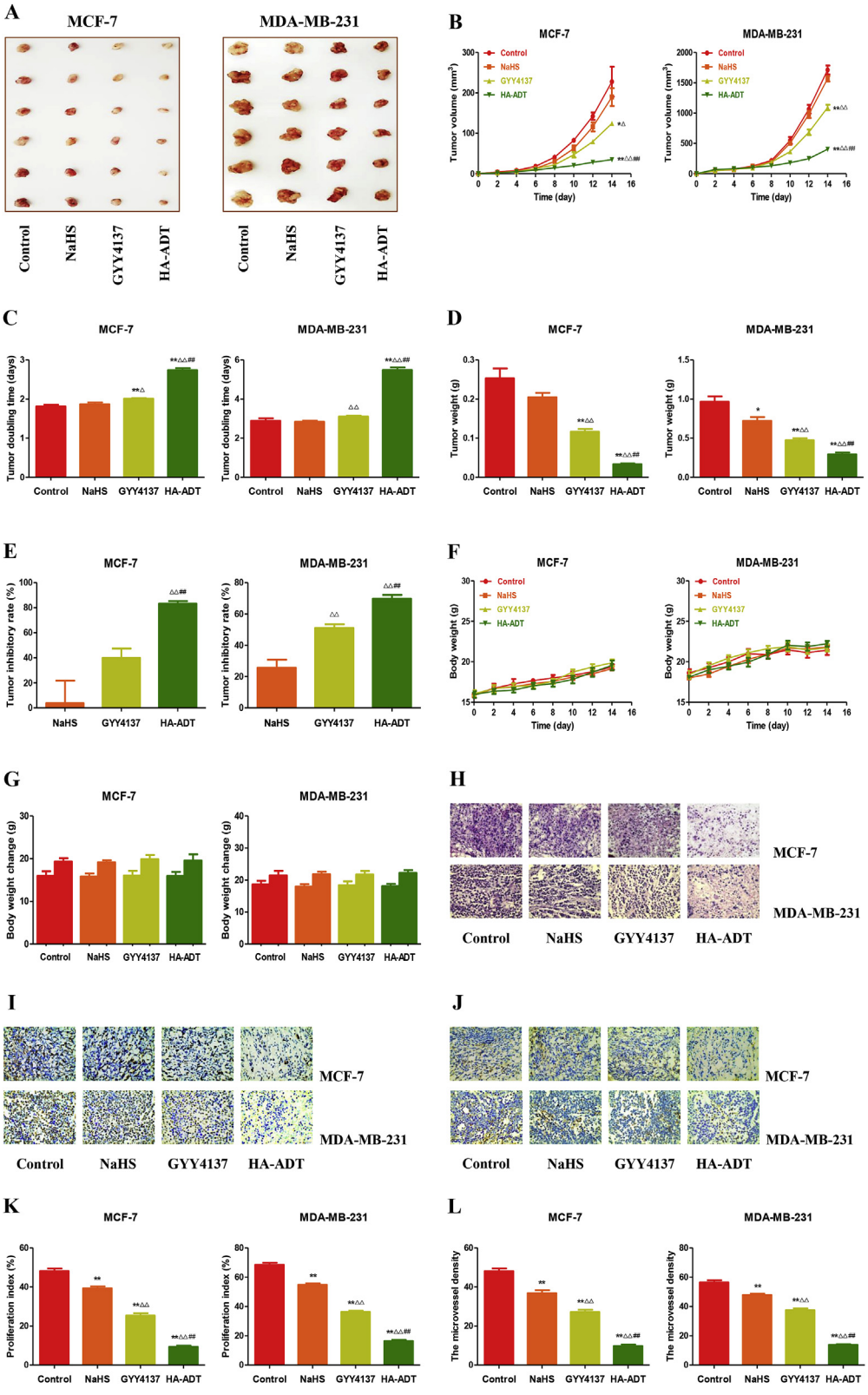


**Fig. 7. Effects of HA-ADT on the growth of MCF-7 and MDA-MB-231 xenograft tumors in nude mice. (A)** Representative xenografts dissected from different groups of nude mice were shown. (**B,C**) The tumor volume of each group was measured every day and the TVDT was calculated by the formula shown above. (**D,E**) The tumors were weighed and the inhibition rates of tumor growth were calculated by the formula shown above. (**F,G**) The body weight change curve of each group during the experiment and the body weight of each group on the first day (day 0) and the last day (day 28). (**H-J**) Representive photographs of HE, Ki67, and CD31 staining in MCF-7 and MDA-MB-231 xenograft tumors; original magnification 400×. (**K,L**) The PI and MVD were calculated by the formula shown above. Values are presented as mean ± SEM (n = 6); $^{*}P < 0.05$, $^{**}P < 0.01$ compared with the control group; $^{\triangle}P < 0.05$, $^{\triangle\triangle}P < 0.01$ compared with NaHS group; $^{\#\#}P < 0.01$ compared with GYY4137 group.

treatment of cancer, such as breast cancer [54–56]. Our results showed that HA-ADT decreased the protein levels of p-PI3K, p-AKT, and p-mTOR, as well as H-RAS, p-RAF, p-MEK, and p-ERK in human breast cancer cells, indicating that HA-ADT could inhibit cell growth and induce apoptosis via blocking the PI3K/AKT/mTOR and RAS/RAF/MEK/ERK signaling pathways in human breast cancer cells.

Recent studies suggest that MCF-7 and MDA-MB-231 cells have been successfully used to establish subcutaneous xenograft models [39,40]. We therefore determined the effects of HA-ADT on the growth of breast cancer xenograft tumors in BALB/c nude mice. Compared with NaHS and GYY4137 group, HA-ADT showed more potent inhibitory effect on the growth of human breast cancer xenograft tumors. In addition, no obvious change was observed in the body weight among each group. In line with the *in vitro* findings, the results showed that the expression of

Ki67 was decreased in the HA-ADT group compared with NaHS and GYY4137 group. Moreover, our results demonstrated that HA-ADT reduced the expression of CD31 in breast cancer xenograft tumors when compared with NaHS and GYY4137 group, indicating that HA-ADT could exert more effective anticancer effects through the suppression of angiogenesis in breast cancer xenograft tumors.

In conclusion, HA-ADT could suppress the growth of human breast cancer cells by inhibiting the PI3K/AKT/mTOR and RAS/RAF/MEK/ERK signaling pathways. HA-ADT and its derivatives might be of great potential in the treatment of different types of cancer.

## Conflicts of interest statement

The authors confirm that there are no conflicts of interest.

## Acknowledgements

This work was supported by grants from the National Natural Science Foundation of China (Nos. 81802718, U1504817, 81670088), the Foundation of Science & Technology Department of Henan Province, China (Nos. 182102310335, 162102410009, 172102410019), the Science Foundation of Kaifeng City, China (Nos. 1608004, 1703016), and the Science Foundation of Henan University, China (No. yqpy20170044).

## Appendix A. Supplementary data

Supplementary data to this article can be found online at https://doi.org/10.1016/j.canlet.2019.04.031.

## References

[1] M. Kwa, A. Makris, F.J. Esteva, Clinical utility of gene-expression signatures in early stage breast cancer, Nat. Rev. Clin. Oncol. 14 (2017) 595–610.
[2] Y. Momozawa, Y. Iwasaki, M.T. Parsons, et al., Germline pathogenic variants of 11 breast cancer genes in 7,051 Japanese patients and 11,241 controls, Nat. Commun. 9 (2018) 4083.
[3] J.A. Sparano, R.J. Gray, D.F. Makower, et al., Adjuvant chemotherapy guided by a 21-gene expression assay in breast cancer, N. Engl. J. Med. 379 (2018) 111–121.
[4] M. Jadaliha, O. Gholamalamdari, W. Tang, et al., A natural antisense lncRNA controls breast cancer progression by promoting tumor suppressor gene mRNA stability, PLoS Genet. 14 (2018) e1007802.
[5] D. Agostini, V. Natalucci, G. Baldelli, et al., New insights into the role of exercise in inhibiting mTOR signaling in triple-negative breast cancer, Oxid Med Cell Longev 2018 (2018) 5896786.
[6] L.S. Cook, C.R. Pestak, A.C. Leung, et al., Combined oral contraceptive use before the first birth and epithelial ovarian cancer risk, Br. J. Canc. 116 (2017) 265–269.
[7] F. Zhang, S. Gong, J. Wu, et al., CXCR4-Targeted and redox responsive dextrin nanogel for metastatic breast cancer therapy, Biomacromolecules 18 (2017) 1793–1802.
[8] M. Li, Z. Tang, D. Zhang, et al., Doxorubicin-loaded polysaccharide nanoparticles suppress the growth of murine colorectal carcinoma and inhibit the metastasis of murine mammary carcinoma in rodent models, Biomaterials 51 (2015) 161–172.
[9] J. Lu, X. Liu, Y.P. Liao, et al., Breast cancer chemo-immunotherapy through liposomal delivery of an immunogenic cell death stimulus plus interference in the Ido-1 pathway, ACS Nano 12 (2018) 11041–11061.
[10] C. Szabo, Gasotransmitters in cancer: from pathophysiology to experimental therapy, Nat. Rev. Drug Discov. 15 (2016) 185–203.
[11] R. Wang, Physiological implications of hydrogen sulfide: a whiff exploration that blossomed, Physiol. Rev. 92 (2012) 791–896.
[12] M.D. Hartle, M.D. Pluth, A practical guide to working with H2S at the interface of chemistry and biology, Chem. Soc. Rev. 45 (2016) 6108–6117.
[13] C. Szabo, C. Coletta, C. Chao, et al., Tumor-derived hydrogen sulfide, produced by cystathionine-β-synthase, stimulates bioenergetics, cell proliferation, and angiogenesis in colon cancer, Proc. Natl. Acad. Sci. U.S.A. 110 (2013) 12474–12479.
[14] J.L. Wallace, R. Wang, Hydrogen sulfide-based therapeutics: exploiting a unique but ubiquitous gasotransmitter, Nat. Rev. Drug Discov. 14 (2015) 329–345.
[15] B.D. Paul, S.H. Snyder, $H_2S$ signalling through protein sulfhydration and beyond, Nat. Rev. Mol. Cell Biol. 13 (2012) 499–507.
[16] N. Shibuya, S. Koike, M. Tanaka, et al., A novel pathway for the production of hydrogen sulfide from D-cysteine in mammalian cells, Nat. Commun. 4 (2013) 1366.
[17] C.R. Powell, K.M. Dillon, J.B. Matson, A review of hydrogen sulfide (H2S) donors: chemistry and potential therapeutic applications, Biochem. Pharmacol. 149 (2018) 110–123.
[18] F. Dosio, S. Arpicco, B. Stella, et al., Hyaluronic acid for anticancer drug and nucleic acid delivery, Adv. Drug Deliv. Rev. 97 (2016) 204–236.
[19] H.S. Jung, W.H. Kong, D.K. Sung, et al., Nanographene oxide-hyaluronic acid conjugate for photothermal ablation therapy of skin cancer, ACS Nano 8 (2014) 260–268.
[20] A. Singh, M. Corvelli, S.A. Unterman, et al., Enhanced lubrication on tissue and biomaterial surfaces through peptide-mediated binding of hyaluronic acid, Nat. Mater. 13 (2014) 988–995.
[21] M.S. Shazeeb, R. Corazzini, P.A. Konowicz, et al., Assessment of in vivo degradation profiles of hyaluronic acid hydrogels using temporal evolution of chemical exchange saturation transfer (CEST) MRI, Biomaterials 178 (2018) 326–338.
[22] U. Hasegawa, A.J. van der Vlies, Design and synthesis of polymeric hydrogen sulfide donors, Bioconjug. Chem. 25 (2014) 1290–1300.
[23] J.W. Bai, M.N. Chen, X.L. Wei, et al., The zinc-finger transcriptional factor Slug transcriptionally downregulates ERα by recruiting lysine-specific demethylase 1 in human breast cancer, Oncogenesis 6 (2017) e330.
[24] G.Y. Zhang, D. Lu, S.F. Duan, et al., Hydrogen sulfide alleviates lipopolysaccharide-induced diaphragm dysfunction in rats by reducing apoptosis and inflammation through ROS/MAPK and TLR4/NF-κB signaling pathways, Oxid Med Cell Longev 2018 (2018) 9647809.
[25] D.D. Wu, Y.R. Gao, T. Li, et al., PEST-containing nuclear protein mediates the proliferation, migration, and invasion of human neuroblastoma cells through MAPK and PI3K/AKT/mTOR signaling pathways, BMC Canc. 18 (2018) 499.
[26] A.M. Heilmann, R.M. Perera, V. Ecker, et al., CDK4/6 and IGF1 receptor inhibitors synergize to suppress the growth of p16INK4A-deficient pancreatic cancers, Cancer Res. 74 (2014) 3947–3958.
[27] B.M. Ellingson, H.N. Nguyen, A. Lai, et al., Contrast-enhancing tumor growth dynamics of preoperative, treatment-naive human glioblastoma, Cancer 122 (2016) 1718–1727.
[28] D. Wu, Y. Gao, L. Chen, et al., Anti-tumor effects of a novel chimeric peptide on S180 and H22 xenografts bearing nude mice, Peptides 31 (2010) 850–864.
[29] B. Keam, S.A. Im, K.H. Lee, et al., Ki-67 can be used for further classification of triple negative breast cancer into two subtypes with different response and prognosis, Breast Cancer Res. 13 (2011) R22.
[30] Y. Liu, S. Jang, L. Xie, G. Sowa, Host deficiency in caveolin-2 inhibits lung carcinoma tumor growth by impairing tumor angiogenesis, Cancer Res. 74 (2014) 6452–6462.
[31] P. Pitchakarn, S. Suzuki, K. Ogawa, et al., Induction of G1 arrest and apoptosis in androgen-dependent human prostate cancer by Kuguacin J, a triterpenoid from Momordica charantia leaf, Cancer Lett. 306 (2011) 142–150.
[32] M. Chen, X. Wang, D. Zha, et al., Apigenin potentiates TRAIL therapy of non-small cell lung cancer via upregulating DR4/DR5 expression in a p53-dependent manner, Sci. Rep. 6 (2016) 35468.
[33] D.A. Fruman, C. Rommel, PI3K and cancer: lessons, challenges and opportunities, Nat. Rev. Drug Discov. 13 (2014) 140–156.
[34] F. Janku, T.A. Yap, F. Meric-Bernstam, Targeting the PI3K pathway in cancer: are we making headway? Nat. Rev. Clin. Oncol. 15 (2018) 273–291.
[35] M. Kitagawa, P.J. Liao, K.H. Lee, et al., Dual blockade of the lipid kinase PIP4Ks and mitotic pathways leads to cancer-selective lethality, Nat. Commun. 8 (2017) 2200.
[36] A.A. Samatar, P.I. Poulikakos, Targeting RAS-ERK signalling in cancer: promises and challenges, Nat. Rev. Drug Discov. 13 (2014) 928–942.
[37] J. Peng, A. Gassama-Diagne, Apicobasal polarity and Ras/Raf/MEK/ERK signalling in cancer, Gut 66 (2017) 986–987.
[38] L. Wan, M. Chen, J. Cao, et al., The APC/C E3 ligase complex activator FZR1 restricts BRAF oncogenic function, Cancer Discov. 7 (2017) 424–441.
[39] R. Scherz-Shouval, S. Santagata, M.L. Mendillo, et al., The reprogramming of tumor stroma by HSF1 is a potent enabler of malignancy, Cell 158 (2014) 564–578.
[40] R. Xu, G. Zhang, J. Mai, et al., An injectable nanoparticle generator enhances delivery of cancer therapeutics, Nat. Biotechnol. 34 (2016) 414–418.
[41] P.C. Adamson, Improving the outcome for children with cancer: development of targeted new agents, Ca - Cancer J. Clin. 65 (2015) 212–220.
[42] C. Robert, V. Sibaud, C. Mateus, et al., Nail toxicities induced by systemic anticancer treatments, Lancet Oncol. 16 (2015) e181–e189.
[43] M. Patra, S.G. Awuah, S.J. Lippard, Chemical approach to positional isomers of glucose-platinum conjugates reveals specific cancer targeting through glucose-transporter-mediated uptake in vitro and in vivo, J. Am. Chem. Soc. 138 (2016) 12541–12551.
[44] E.C. Calvaresi, P.J. Hergenrother, Glucose conjugation for the specific targeting and treatment of cancer, Chem. Sci. 4 (2013) 2319–2333.
[45] E.A. Akam, E. Tomat, Targeting iron in colon cancer via glycoconjugation of thiosemicarbazone prochelators, Bioconjug. Chem. 27 (2016) 1807–1812.
[46] D. Wu, W. Si, M. Wang, et al., Hydrogen sulfide in cancer: friend or foe? Nitric Oxide 50 (2015) 38–45.
[47] D. Wu, Y. Gao, Y. Qi, et al., Peptide-based cancer therapy: opportunity and challenge, Cancer Lett. 351 (2014) 13–22.
[48] W. Ju, M. Zhang, K.M. Wilson, et al., Augmented efficacy of brentuximab vedotin combined with ruxolitinib and/or Navitoclax in a murine model of human Hodgkin's lymphoma, Proc. Natl. Acad. Sci. U.S.A. 113 (2016) 1624–1629.
[49] P. De Cicco, E. Panza, G. Ercolano, et al., ATB-346, a novel hydrogen sulfide-releasing anti-inflammatory drug, induces apoptosis of human melanoma cells and inhibits melanoma development in vivo, Pharmacol. Res. 114 (2016) 67–73.
[50] J. Rodon, R. Dienstmann, V. Serra, et al., Development of PI3K inhibitors: lessons learned from early clinical trials, Nat. Rev. Clin. Oncol. 10 (2013) 143–153.
[51] C.H. Sun, Y.H. Chang, C.C. Pan, Activation of the PI3K/Akt/mTOR pathway correlates with tumour progression and reduced survival in patients with urothelial carcinoma of the urinary bladder, Histopathology 58 (2011) 1054–1063.
[52] R. Mandal, S. Becker, K. Strebhardt, Stamping out RAF and MEK1/2 to inhibit the

ERK1/2 pathway: an emerging threat to anticancer therapy, Oncogene 35 (2016) 2547–2561.
[53] Y. Wang, H. Nie, X. Zhao, et al., Bicyclol induces cell cycle arrest and autophagy in HepG2 human hepatocellular carcinoma cells through the PI3K/AKT and Ras/Raf/MEK/ERK pathways, BMC Canc. 16 (2016) 742.
[54] T. Shimizu, A.W. Tolcher, K.P. Papadopoulos, et al., The clinical effect of the dual-targeting strategy involving PI3K/AKT/mTOR and RAS/MEK/ERK pathways in patients with advanced cancer, Clin. Cancer Res. 18 (2012) 2316–2325.
[55] E. Jokinen, N. Laurila, J.P. Koivunen, Alternative dosing of dual PI3K and MEK inhibition in cancer therapy, BMC Canc. 12 (2012) 612.
[56] K.S. Saini, S. Loi, E. de Azambuja, et al., Targeting the PI3K/AKT/mTOR and Raf/MEK/ERK pathways in the treatment of breast cancer, Cancer Treat Rev. 39 (2013) 935–946.